Late Pleistocene glacial fluctuations in Cordillera Oriental, subtropical Andes

Mateo A. Martini [a, *], Michael R. Kaplan [b], Jorge A. Strelin [a, c], Ricardo A. Astini [a], Joerg M. Schaefer [b, d], Marc W. Caffee [e, f], Roseanne Schwartz [b]

[a] Centro de Investigaciones en Ciencias de la Tierra (CONICET-UNC), Vélez Sársfield 1611, X5016GCA, Córdoba, Argentina
[b] Geochemistry, Lamont-Doherty Earth Observatory, Palisades, NY 10964, USA
[c] Instituto Antártico Argentino, Convenio MREC - Universidad Nacional de Córdoba, Vélez Sársfield 1611, X5016GCA, Córdoba, Argentina
[d] Department of Earth and Environmental Sciences, Columbia University, New York, NY 10027, USA
[e] Department of Physics and Astronomy, Purdue University, West Lafayette, IN 47907, USA
[f] Department of Earth, Atmospheric, and Planetary Sciences, Purdue University, West Lafayette, IN 47907, USA

ARTICLE INFO

ABSTRACT

The behavior of subtropical glaciers during Middle to Late Pleistocene global glacial maxima and abrupt climate change events, specifically in Earth's most arid low-latitude regions, remains an outstanding problem in paleoclimatology. The present-day climate of Cordillera Oriental, in arid northwestern Argentina, is influenced by shifts in subtropical climate systems, including the South American Summer Monsoon. To understand better past glacier-subtropical climates during the global Last Glacial Maximum (LGM, 26.5–19 ka) and other time periods, we combined geomorphic features with forty-two precise ^{10}Be ages on moraine boulders and reconstructed paleo-equilibrium line altitudes (ELA) at Nevado de Chañi (24°S) in the arid subtropical Andes. We found a major glacial expansion at ~23 ± 1.6 ka, that is, during the global LGM. Additional glacial expansions are observed before the global LGM (at ~52–39 ka), and after, at 15 ± 0.5 and 12 ± 0.6 ka. The ~15 ka glacial event was found on both sides of Chañi and the ~12 ka event is only recorded on the east side. Reconstructed ELAs of the former glaciers exhibit a rise from east to west that resembles the present subtropical climate trajectory from the Atlantic side of the continent; hence, we infer that this climate pattern must have been present in the past. Based on comparison with other low-latitude paleoclimate records, such as those from lakes and caves, we infer that both temperature and precipitation influenced past glacial occurrence in this sector of the arid Andes. Our findings also imply that abrupt deglacial climate events associated with the North Atlantic, specifically curtailed meridional overturning circulation and regional cooling, may have had attendant impacts on low subtropical Southern Hemisphere latitudes, including the climate systems that affect glacial activity around Nevado de Chañi.

1. Introduction

Present-day glaciers in the Andes exist under diverse climatic conditions (Lliboutry, 1999; Sagredo and Lowell, 2012). In the driest part of the Chilean Andes, between 18°30' and 27°S, no present-day glaciers are found due primarily to extreme aridity (Ammann et al., 2001; Casassa et al., 2007). Moreover, between 25 and 27°S, there is no clear evidence of former glaciers during the late Quaternary inclusive of ranges as high as 6000 m asl (Ammann et al., 2001).

This particularity makes the subtropical arid Andes a special place to study the present and former evolution of the cryosphere, and in particular the glacial evolution during the last glaciation. Several lines of evidences support the existence of cooling and phases of higher precipitation during the last 130 ka producing, among other changes, the expansion of large lakes on the Altiplano (Baker et al., 2001b; Placzek et al., 2006; 2013; Blard et al., 2011). Such climatic, including hydrologic, variations have impacted the landscape due to the enhancement of surface processes such as landslides (Trauth et al., 2000, 2003; Hermanns et al., 2006). The Late Pleistocene glacier chronology in the subtropical Andes is not precisely constrained on a regional spectrum to evaluate the influence of such

past climate changes. Given the lack of age control along the subtropical Andes, more geochronological data are needed on glacial deposits in order to have a better understanding of such relationships, and to strengthen glacial-climate reconstructions based on geomorphologic evidence (e.g., Porter, 2001; Ammann et al., 2001; Haselton et al., 2002).

Furthermore, in tropical to subtropical South America, questions remain on past climate regime shifts during glacial-ages, including changes in the Intertropical Convergence Zone (ITCZ) and the midlatitude Southern Hemisphere Westerlies, as well as the relative importance of far-field influences such as polar and North Atlantic conditions (Denton et al., 2010; Baker and Fritz, 2015). It is unclear how the South American Summer Monsoon (SASM) responded to these low-latitude and far-field influences, especially during the global Last Glacial Maximum (LGM) (26.5—19 ka; Clark et al., 2009) and during abrupt climate changes that are seen in both polar ice-cores and high latitude ocean records in the North and South Hemispheres (Barker et al., 2009; Pedro et al., 2011; Members, 2015). Some works pointed out the link between North Atlantic cooling and the SASM was enhanced in the Amazonas region and Central Andes during the last glacial to interglacial period (Wang et al., 2004, 2007; Quade et al., 2008; Blard et al., 2011; Kanner et al., 2012; Placzek et al., 2013; Stríkis et al., 2015). This is a mechanism by which climate drivers far outside South America (e.g., Northern Hemisphere ice sheets) can have a major impact on its glacier and geomorphic history. However, it remains unclear to what extent the SASM may have shifted southward, especially at high-altitude sites in the subtropical Andes, and affected the glaciers.

Subtropical glacier records and their chronologies can substantially improve our knowledge of past atmospheric climate dynamics (mainly temperature and precipitation) to address the issues above. The Cordillera Oriental of Argentina is an excellent place for studying how glaciations and other morphoclimatic process manifest themselves in Earth's arid subtropical settings, and for characterizing their changes during the abrupt switch to the warmer interglacial, after the global LGM. Its location is particularly significant, being in a part of the continent where the interaction between the SASM and the South American Low Level Jet (SALLJ) dictates the climate (Garreaud et al., 2009; Vuille et al., 2012). Therefore, it is ideally situated to test the influence of the SASM on

glacial activity during the Late Pleistocene.

In this work, we analyze the glacial geomorphology of the Nevado de Chañi massif (Fig. 1), located on the arid subtropical eastern slope of the Central Andes and we establish a new chronology based on high precision cosmogenic [10]Be surface dating. To evaluate the moisture trajectory during glaciations we reconstruct glacier paleo-equilibrium line using several newly-dated moraines. Finally, we compare and review the new glacial history with other paleoclimatic proxies and discuss local and global implications.

2. Regional settings

The Cordillera Oriental of Argentina is located on the eastern border of Puna-Altiplano, on the northeast side of the low-precipitation (less than 250 mm/yr) narrow band, the so-called Arid Diagonal. This is a major climatic boundary with a southeast-northwest trend, which crosses the Andes between 25° and 27°S (Fig. 1). Most of the annual precipitation (~75%) in Cordillera Oriental takes place during the austral summer (from December to March) and is related to the SASM (Zhou and Lau, 1998).

Specifically, during the austral spring the ITCZ migrates southward and produces the onset of the SASM in response to the thermal contrast between the continent and the adjacent ocean (Vera, 2006). The SASM reaches its mature phase between December and February. The dynamics of the ITCZ affect the SASM intensity and therefore the moisture influx and overall climate conditions to this part of the continent (Vuille et al., 2012), a circumstance that is important for this investigation. A deep continental low forms over the Chaco region (25°S) and forces the easterly winds to turn southward and transport significant amounts of moisture across the SALLJ from the Amazon region into the northwestern Argentina (Garreaud et al., 2009), including areas of our focus (Fig. 1). The winds and weather from the east-northeast create an orographic effect across the Cordillera Oriental (Bianchi and Yañez, 1992), with a much drier western side, which is reflected in the regional-scale geomorphic evolution (Strecker et al., 2007) (Fig. 1). Only the highest peak of the Cordillera Oriental of Argentina, the Nevado de Cachi (6380 m above sea level (asl)) contains glaciers. There are four small glaciers (less than 1 km²), which are situated above 5600 m asl (Martini et al., 2013). Based on
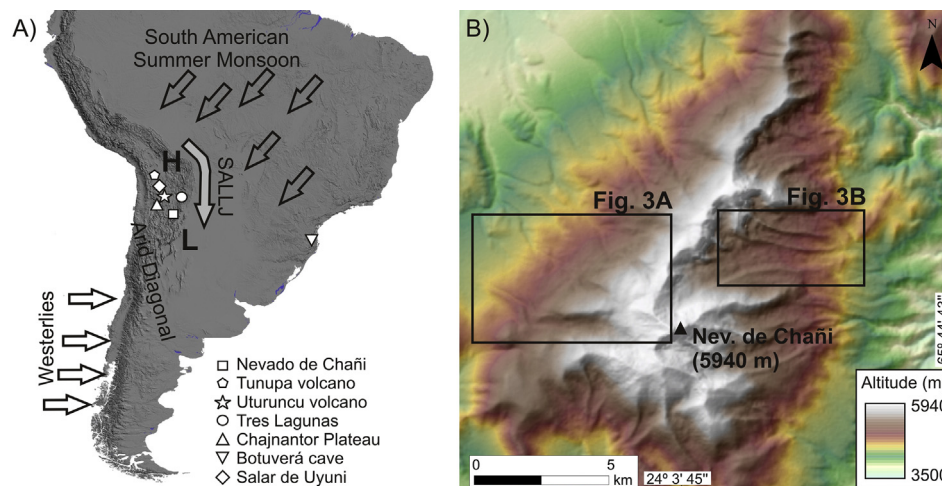
Fig. 1. (A) Mean atmospheric circulations patterns in South America. SALLJ: South American Low Level Jet; H: Bolivian High; L: Chaco Low. Arrows in low and high latitude South America denote the mean wind director at 925 hPa. Symbols indicate the locations of prior works mentioned in the text: Nevado de Chañi (this work), Tunupa volcano (Clapperton et al., 1997; Blard et al., 2009, 2013a), Uturuncu volcano (Blard et al., 2014), Tres Lagunas (Zech et al., 2009), Chajnantor Plateau (Ward et al., 2015), Botuverá cave (Wang et al., 2007), Salar de Uyuni (Placzek et al., 2006). (B) Digital Elevation Model of the Nevado de Chañi massif with the location of Fig. 3. Note the difference in slope and relief between the east and west side.

their size, the location, and the regional climatic conditions, they are classified as reservoir glaciers (*cf.* Lliboutry, 1956). This variety of glacier is typical in the dry high-altitude Andes, where they are situated far above the 0 °C isotherm altitude, they do not have considerable flow, and the annual mass balance is similar across the whole area of the glacier (not altitude-dependent) (Milana, 2012).

The Nevado de Chañi (5940 m asl), which is the focus of this study, is a north-south trending mountain range situated in the central part of the Cordillera Oriental (Fig. 1). The west side of Nevado de Chañi drains into the closed-watershed of Salinas Grandes in the Puna-Altiplano and the east side is part of the Bermejo watershed, which drains into the Atlantic Ocean. The east-west asymmetry found in the Cordillera Oriental is also present at Nevado de Chañi (Figs. 2 and 3), where the east side contains higher relief and steeper slopes than the west side. The Nevado de Chañi is composed of Precambrian and Paleozoic sedimentary rocks (metasedimentary and sandstones) intruded by Cambrian granites (González et al., 2004; Zappettini et al., 2008). Glacigenic deposits and erosional landforms evince the presence of glaciers during the Late Pleistocene (Martini et al., 2015). At present, above 4500 m a.s.l. periglacial activity takes a main role in the development of the landscape (Martini et al., 2013). Based on the La Quiaca weather station located ~210 km north of Nevado de Chañi, the regional 0 °C isotherm is estimated to be ~4910 m asl (Martini et al., 2013). We also installed an automatic meteorological station at 4910 m asl on Nevado de Chañi. For 2012, the mean annual air temperature was 1.3 °C and we assume the annual 0 °C isotherm was slightly higher. Although the highest part of Nevado de Chañi is located above the

Fig. 2. The west (A) and east (B) sides of Nevado de Chañi. Note the slope and relief differences. The arrows indicate the highest part of the range (5882 m asl).

0 °C isotherm, no glaciers exist today. The reasons include a dry climate with a mean annual precipitation less than 400 mm, and intense solar radiation at high elevations, which causes high summer ablation rates, as in others sectors of the subtropical Central Andes (e.g., Schotterer et al., 2003; Vargo and Galewsky, 2014).

3. Methods

3.1. Mapping and sample collection

Using satellite images, aerial photographs, and a digital elevation model we mapped the main glacial and periglacial landforms on both sides of the Nevado de Chañi (Fig. 3). We carried out 4 field seasons to check the interpretations made for the map. We grouped lateral, frontal and central moraines into five different Moraine Groups (MG I to V) on the basis of their position, morphology, and chronology. We collected 42 samples from erratic boulders situated on moraines crests for cosmogenic [10]Be surface exposure dating (e.g., Figs. 4 and 5). The moraine crest marks the former position of the glacier margin, which could represent either a stillstand or the culmination of an advance (e.g., Putnam et al., 2013). We infer the cosmogenic [10]Be ages from moraine boulders on crest tops date relatively close to the end of the causal climate event or onset of withdrawal of the ice margin from the landform.

The samples were taken with hammer and chisel from the top 1–3 cm, from well-preserved flat surfaces on erratic boulders. Some of the boulders sampled contain striations, showing signs of little or no postglacial erosion. The sampled litholgies include hard quartz-rich granites (Chañi Formation) and quartzitic sandstones (Meson Group) (González et al., 2004) (Table 1). The location and altitude of each sample were measured using Trimble ProXH or R4 GPS system and were corrected differentially using the Salta city permanent GPS station. Post-processed uncertainties (1σ) for the samples were less than 0.6 m in the altitudinal and less than 0.4 m in the horizontal.

3.2. [10]Be surface-exposure dating

We use recent advances in [10]Be dating that allow improved precision (analytical uncertainties are less than 4% and typically 2%) compared with prior studies in central South America (Zech et al., 2009; Ward et al., 2015) (Table 1). Samples were prepared in the Cosmogenic Nuclide Laboratory at the Lamont-Doherty Earth Observatory following the methods of Schaefer et al. (2009) and, [10]Be/[9]Be ratios were measured at PRIME Lab or at the Center for Accelerator Mass Spectrometry at Lawrence Livermore National Laboratory. [10]Be/[9]Be was measured relative to the 07KNSTD AMS standard (Nishiizumi et al., 2007). The [10]Be/[9]Be ratio of sample CH-10-86 was measured twice and the sample age was calculated using the average of the two results. During the processing, we used one procedural blank for each batch of samples (n = 7–10). The concentration of the procedural blank was subtracted from the [10]Be concentration of the respective samples. In all the cases the blank corrections represent less than 0.2% the sample measurement. The exposures ages were calculated using CRONUS-Earth online calculator (Version 2.2; Balco et al., 2008). We used a rock density of 2.65 g/cm^{3}. No erosion was considered in the age calculations because we did not find clear evidence on the surfaces sampled and the highly resistant lithologies are not prone to erode. We also did not consider shielding by snow accumulation on the boulders because present-day (<400 mm/yr; Bianchi and Yañez, 1992), and we assume also past, precipitation is insignificant on top of moraine crests in terms of long-term integrated exposure history, in this arid environment. We also noted that no snow accumulation on the ground was registered by a weather station located at 4910 m asl on
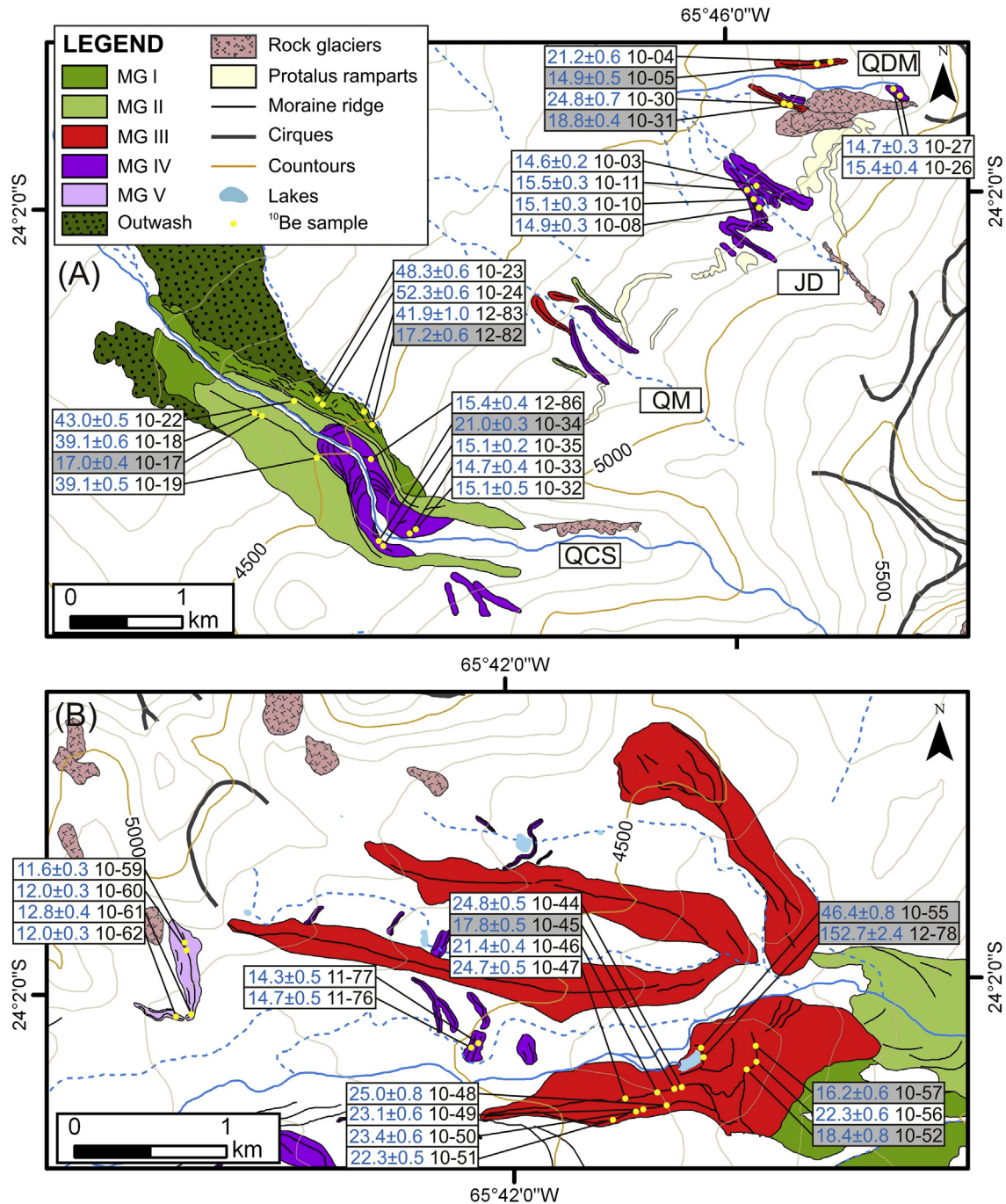
Fig. 3. Glacial geomorphological maps of the west (A) and east (B) sides of Nevado de Chañi (see Fig. 1 for location). Shown are ¹⁰Be ages (blue text) and the last 4 digits of the sample ID (black text). Grey boxes represent outliers. Ages are in ka, with ±1σ analytical (internal) uncertainty. QCS: Quebrada Chañi Sur valley, QDM: Quebrada del Medio valley, JD: Jefatura de Diablos valley, QM Quebrada de la Mina valley. Fig. 3B shows only the Refugio valley. (For interpretation of the references to colour in this figure legend, the reader is referred to the web version of this article.)

Nevado de Chañi over 16 months of observations.

The exposure ages were calculated using the regional high-altitude low-latitude production rate of Kelly et al. (2015) for the subtropical Andes (Peru), which is statistically identical, within uncertainties, to other South American and Southern Hemisphere rates (Blard et al., 2013b; Martin et al., 2015; Kaplan et al., 2011; Putnam et al., 2010). The difference using the two Southern Hemisphere high-altitude and low-latitude production rates available in the CRONUS-Earth online calculator is ≤ 5% (i.e., Kelly et al., 2015; Blard et al., 2013b). We use the regional production rate of Kelly et al. (2015) because it is within the same high elevation range (4350–4850) of our samples (Table 1) and it is more precise (±2.4%) than the Blard et al. (2013b) production rate (3800 m asl; ±6.1%), although both are statistically identical. In the text, the ages discussed are based on the time-dependent Stone-Lal ('Lm') scaling (Balco et al., 2008). We use the 'Lm' (time-dependent Stone, 2000/Lal, 1991) and 'St' (Stone, 2000) scaling schemes because neutron-monitor based scaling frameworks have much poorer fit to the primary calibration data sets (Lifton et al., 2014; Borchers et al., 2016). The difference using 'St' or 'Lm' scaling
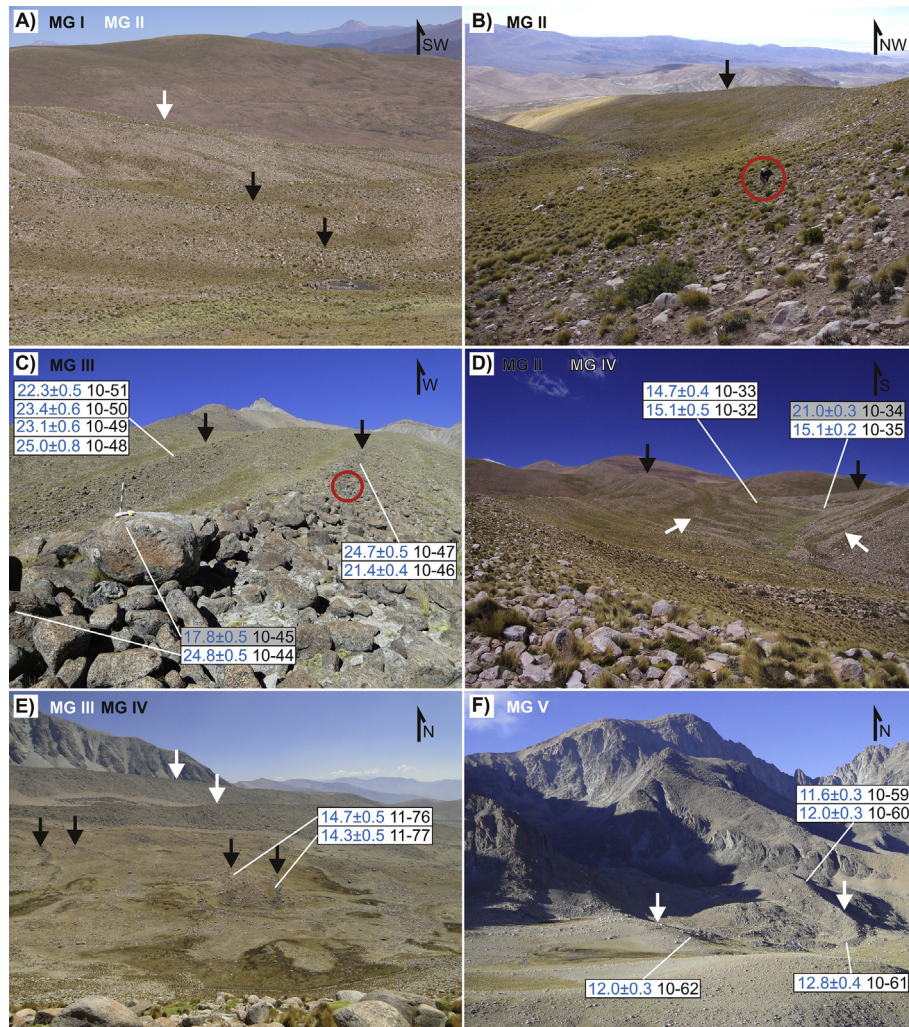
Fig. 4. Field photos of the different moraine groups. A) MG I and II on the west side. B) Lateral moraine of MG II on the west side. C) Lateral moraines of MG III on the east side. D) Lateral moraines of MG II and lateral/frontal moraines of MG IV on the west side. E) MG IV and the central moraines of MG III on the east side. F) MG V on the east side which is near the headwall. The black and white arrows point to the different MG respectively. The red circles highlight a person for scale. In the upper right corner of each photo is the direction of the view. Boulders ages (±1σ in ka) and sample ID (last 4 digits) are shown with dark boxes representing outliers. (For interpretation of the references to colour in this figure legend, the reader is referred to the web version of this article.)

scheme changes the ages by ≤ 5% for LGM time, ≤2% for Lateglacial time and ≤22% for pre-LGM time. Therefore, the choice of scaling scheme or Southern Hemisphere production rate does not affect our main interpretations and conclusions. To compare our mean moraine ages with the timing of other proxy changes, we also propagate a production rate uncertainty (±2.4%; Kelly et al., 2015).

3.3. Equilibrium line altitude reconstructions

Paleo-equilibrium line altitudes (ELA) were estimated for MG III, IV, and V on the east side and for MG IV on the west side using the Accumulation Area Ratio (AAR) method (Porter, 1975). To reconstruct the ELA of former glaciers, we first delimit the glacier extent, using moraine crests in the ablation zone and erosional features in the accumulation zone as glacier limits. We then reconstruct the glacier surface elevation taking some control points (e.g., moraine crest) that mark the glacier position and draw its surface with a contour interval of 50 m (Fig. 6). The contour levels were drawn concave in near the accumulation zone and convex in near the ablation zone, and perpendicular with respect to the inferred paleoglacier flow direction. Then, we construct the hypsometric

curve of the glacier (cumulative area vs altitude) and extract the paleo-ELA from 67% of the area counting from the accumulation area (i.e. AAR = 0.67) (Fig. 6). An AAR = 0.67 was used because this represents the average for Bolivian glaciers (Jordan, 1991). Slight changes in assumed AAR should not significantly affect our conclusions, as we focus mainly on the relative changes between events (e.g., Fig. 3B). For each paleo-ELA we estimated an error equal to the contour interval (±50 m).

4. Results

4.1. Geomorphology and moraine sequences

The present-day climatic and geomorphologic asymmetry between the east and west sides of Nevado de Chañi are also reflected in the respective MG crests, which have different relative sizes on both sides (Figs. 2–4). MG I represents the most extended and oldest moraine group. On the east side, its crests are found above 3790 m asl and they have been partially removed by fluvial erosion. On the west side, MG I crests are restricted to the Quebrada Chañi Sur valley where they are found above 4150 m asl (Fig. 4).

Fig. 5. Photos showing examples of boulders sampled for [10]Be exposure dating with the age (±1σ in ka), and sample ID (last 4 digits) in the box.

Associated with MG I is a downstream outwash plain.

On both sides of Nevado de Chañi, MG I is partially overridden by MG II (Figs. 3 and 4). On the east side, MG II consists of small parallel ridges. On the west side, in the Quebrada Chañi Sur valley, MG II consists of two sharp lateral moraines more than 50 m in height that draw near downstream, which are located above 4270 m asl.

MG III is well developed in all valleys on the east side. In the Refugio valley, it lies above 4110 m asl and its frontal moraine is more than 70 m in height. Lateral moraines are found in the south sector of the valley and are composed of two main crests (Figs. 3 and 4) that join to the terminal moraine. Just slightly farther inboard, two sharp crests of central moraines are also mapped as MG III given similar elevations and geomorphologic characteristics (Fig. 3). On the west side, MG III moraines occupy a much smaller area compared to the east side. They are located above 4615 m asl, close to MG IV (Fig. 3). In the Quebrada Chañi Sur valley, MG III is not present.

MG IV is well represented in many valleys on both sides of Nevado de Chañi. On the west side, when they are observed, MG IV moraines are close to MG IIII. In the Quebrada Chañi Sur valley, MG IV consists of more than eight parallel moraines deposited near the valley bottom (Fig. 4). In Jefatura de Diablos valley these moraines are thicker (~20 m), whereas in the Quebrada de la Mina they are mainly represented by erratic boulders scattered in the valley bottom. On the east side, they are located ~1.5 km upstream from the frontal moraine of the older MG III (Figs. 3 and 4). Here, MG IV consists of sharp and continuous, typically less than 6 m high, parallel moraines found in the bottom of the valleys. We interpreted MG IV as indicating stabilization interrupting overall recession during the glacial to interglacial transition, which is supported by the subsequently-obtained age constraints.

Situated inboard of MG IV, MG V is restricted to the east side of Nevado de Chañi (Fig. 3B). It consists of continuous sharp lateral and frontal moraine crest located above 4650 m asl, and contains hard resistant granite boulders (Figs. 4 and 5). It represents the innermost and, therefore, the youngest moraine group. After MG V,

no glacial advances are observed in the Nevado de Chañi.

4.2. Boulders exposure ages and moraine group chronologies

Due to potential geomorphic processes, outliers may be expected from erratic boulders on the same moraine crest or moraine system. For example, younger ages than that of moraine deposition can be due to post-depositional processes such as shielding of the sampled surface (e.g., within the moraine) and its subsequent exhumation, boulder erosion (e.g., spallation), or boulder rotation with a subsequent change of the surface exposed. Also, it is possible that some boulders have apparent ages older than that of moraine deposition, due to previous exposure (inheritance). Outside the polar regions where cold-based glaciers are common, post-depositional processes are generally more important than pre-exposure as agents for the scattering of ages on glacial deposits older than the Holocene (e.g., in South America, Douglass et al., 2006; Kaplan et al., 2007; in New Zealand, Putnam et al., 2013).

4.2.1. MG I and II

For MG I and II on the west side (no ages were obtained on the east side), 6 of 8 boulders have exposure ages that ranges from 52.3 to 39.1 ka (Figs. 3 and 5). Two boulders (CH-10-17 and CH-12-82), one on MG I and one on MG II, have an age of ~17 ka. Despite the coherent ages of these two younger boulders with each other, it is unlikely that they represent the age of MG I and II because they contradict the other 6 ages, and perhaps most important the MG I ~17 ka boulder violates the relative stratigraphy of almost all ages (except one) of the inboard and thus younger MG II (Fig. 3A). The youngest sample of MG II (CH-10-17 of age 17 ± 0.4 ka) does not violate relative stratigraphy. However, we consider it improbable one out of the four ages on MG II represents the true age of the moraine given that the three remaining ages range from ~43 to ~39 ka. It is possible that these two samples (CH-10-17 and CH-12-82) represent post-depositional processes, such as boulder disturbance, and we considered them as outliers at least in the context of the 8 ages. We did not find obvious signs of erosion on the sampled

Table 1
Geographical and analytical sample data. The ^{10}Be/^{9}Be ratio of sample CH-10-86 was measured twice. Ages were calculated using Kelly et al. (2015) production rate and the time-dependent Stone-Lal ('Lm') scaling (Balco et al., 2008). MG: Moraine Group.

Sample ID	Latitude (°S)	Longitude (°W)	Altitude (m a.s.l.)	Boulder size (L × W × H) (m)			Lithology	Sample thickness (cm)	Shielding correction	^{10}Be/^{9}Be ±1σ (10^{-14})	^{10}Be ±1σ (10^4 atoms g^{-1})	Age ±1σ[a] (ka)	MG
CH-12-83	−24.04969	−65.79930	4493	2.0	1.9	1.2	Granite	1.0	0.998	73.00 ± 0.02	222.92 ± 5.23	41.9 ± 1.0	I
CH-10-23	−24.04803	−65.80363	4418	4.7	3.1	2.0	Granite	1.7	0.999	240.77 ± 3.18	250.46 ± 3.31	48.3 ± 0.6	I
CH-10-24	−24.04823	−65.80346	4422	1.3	0.8	1.3	Granite	1.9	0.999	262.02 ± 2.89	267.91 ± 2.95	52.3 ± 0.6	I
CH-12-82	−24.05005	−65.79916	4490	2.0	1.1	1.3	Sandstone	0.8	0.997	26.00 ± 0.01	78.50 ± 2.74	17.2 ± 0.6	I
CH-10-18	−24.05021	−65.80857	4387	3.4	2.5	1.8	Granite	0.7	0.999	184.21 ± 2.93	195.83 ± 3.12	39.1 ± 0.6	II
CH-10-19	−24.05398	−65.80313	4513	2.7	1.1	1.1	Granite	1.6	0.999	196.94 ± 2.39	206.16 ± 2.51	39.1 ± 0.5	II
CH-10-22	−24.04911	−65.80525	4420	4.4	1.4	1.4	Granite	0.8	0.999	214.74 ± 2.46	224.22 ± 2.57	43.0 ± 0.5	II
CH-10-17	−24.05039	−65.80813	4393	4.1	2.5	1.3	Granite	0.6	0.998	72.15 ± 1.67	74.87 ± 1.73	17.0 ± 0.4	II
CH-10-48	−24.04086	−65.69206	4454	5.5	4.0	1.8	Granite	0.9	0.998	38.40 ± 0.01	117.42 ± 3.68	25.0 ± 0.8	III
CH-10-30	−24.02641	−65.76001	4725	1.5	0.9	0.6	Sandstone	1.8	0.992	86.02 ± 0.02	130.34 ± 3.71	24.8 ± 0.7	III
CH-10-44	−24.03942	−65.68833	4378	2.0	1.9	1.0	Granite	0.9	0.998	37.90 ± 0.01	112.48 ± 2.38	24.8 ± 0.5	III
CH-10-47	−24.03985	−65.69128	4415	2.5	2.0	1.3	Granite	1.0	0.998	40.60 ± 0.01	113.82 ± 2.25	24.7 ± 0.5	III
CH-10-50	−24.04071	−65.69107	4428	1.4	0.9	1.0	Granite	0.9	0.998	38.20 ± 0.01	107.96 ± 2.55	23.4 ± 0.6	III
CH-10-49	−24.04072	−65.69112	4431	3.0	2.5	1.6	Granite	2.4	0.998	34.60 ± 0.01	105.05 ± 2.75	23.1 ± 0.6	III
CH-10-56	−24.03807	−65.68408	4351	2.5	1.8	1.3	Granite	0.9	0.998	32.00 ± 0.01	97.99 ± 2.78	22.3 ± 0.6	III
CH-10-51	−24.04052	−65.68919	4383	3.9	2.5	1.5	Granite	1.0	0.996	33.10 ± 0.01	99.49 ± 2.11	22.3 ± 0.5	III
CH-10-46	−24.03947	−65.68879	4380	1.6	1.4	0.9	Granite	1.2	0.997	31.00 ± 0.01	95.48 ± 1.85	21.4 ± 0.4	III
CH-10-04	−24.02245	−65.75677	4768	2.0	1.7	1.2	Granite	0.9	0.995	67.37 ± 0.02	112.25 ± 3.16	21.2 ± 0.6	III
CH-10-31	−24.02645	−65.75995	4725	0.8	0.7	0.5	Sandstone	0.7	0.995	43.94 ± 0.01	96.72 ± 1.93	18.8 ± 0.4	III
CH-10-52	−24.03928	−65.68477	4341	3.3	1.9	1.1	Granite	1.0	0.998	26.00 ± 0.01	78.88 ± 3.36	18.4 ± 0.8	III
CH-10-45	−24.03942	−65.68833	4378	1.7	1.7	1.3	Granite	0.9	0.998	26.00 ± 0.01	77.51 ± 2.10	17.8 ± 0.5	III
CH-10-57	−24.03708	−65.68405	4349	2.4	1.9	1.6	Granite	0.7	0.998	23.00 ± 0.01	68.36 ± 2.43	16.2 ± 0.6	III
CH-10-05	−24.02268	−65.75760	4777	1.5	0.9	0.9	Sandstone	2.2	0.995	50.17 ± 0.02	75.78 ± 2.58	14.9 ± 0.5	III
CH-10-55	−24.03724	−65.68725	4347	2.9	2.1	1.6	Granite	1.5	0.998	78.00 ± 0.01	233.73 ± 4.20	46.4 ± 0.8	III
CH-12-78	−24.03837	−65.68727	4366	1.6	1.1	0.9	Granite	0.8	0.998	251.30 ± 0.04	769.10 ± 12.26	152.7 ± 2.4	III
CH-12-86A	−24.05386	−65.79906	4561	1.0	0.8	0.8	Sandstone	1.7	0.997	45.41 ± 0.01	69.92 ± 1.50	15.1 ± 0.3	IV
CH-12-86B	−24.05386	−65.79906	4561	1.0	0.8	0.8	Sandstone	1.7	0.997	53.59 ± 0.02	73.35 ± 2.57	15.7 ± 0.6	IV
CH-10-11	−24.03317	−65.76486	4742	1.3	1.2	1.0	Sandstone	1.2	0.995	35.58 ± 0.01	78.48 ± 1.62	15.5 ± 0.3	IV
CH-10-26	−24.02507	−65.75166	4849	1.8	1.4	0.8	Sandstone	0.9	0.983	37.02 ± 0.01	80.89 ± 1.84	15.4 ± 0.4	IV
CH-10-32	−24.05998	−65.79493	4635	2.3	1.5	0.9	Granite	0.9	0.996	32.80 ± 0.01	73.43 ± 2.23	15.1 ± 0.5	IV
CH-10-10	−24.03383	−65.76444	4761	1.4	0.8	0.8	Sandstone	0.6	0.996	34.86 ± 0.01	77.28 ± 1.75	15.1 ± 0.3	IV
CH-10-35	−24.06069	−65.79797	4618	3.2	2.0	1.1	Granite	0.6	0.993	91.43 ± 1.25	72.21 ± 0.99	15.1 ± 0.2	IV
CH-10-08	−24.03478	−65.76385	4805	1.8	1.3	1.0	Sandstone	1.1	0.992	34.92 ± 0.01	76.98 ± 1.62	14.9 ± 0.3	IV
CH-10-27	−24.02564	−65.75062	4847	4.3	1.8	1.3	Sandstone	1.5	0.983	211.45 ± 4.07	76.85 ± 1.48	14.7 ± 0.3	IV
CH-10-33	−24.06010	−65.79499	4631	2.2	1.3	1.0	Granite	1.0	0.996	32.70 ± 0.01	70.90 ± 1.74	14.7 ± 0.4	IV
CH-10-03	−24.03306	−65.76376	4758	2.3	1.1	1.0	Sandstone	3.1	0.995	70.75 ± 0.97	72.94 ± 1.00	14.6 ± 0.2	IV
CH-11-76	−24.03704	−65.70259	4500	2.8	2.7	3.2	Granite	1.5	0.996	21.70 ± 0.01	66.74 ± 2.45	14.7 ± 0.5	IV
CH-11-77	−24.03720	−65.70222	4495	4.2	2.7	2.3	Granite	1.0	0.994	21.10 ± 0.01	67.48 ± 2.14	14.3 ± 0.5	IV
CH-10-34	−24.06069	−65.79803	4620	4.8	2.7	1.2	Granite	0.7	0.993	132.92 ± 1.82	103.79 ± 1.42	21.0 ± 0.3	IV
CH-10-61	−24.03473	−65.72081	4662	2.9	1.8	1.5	Granite	1.8	0.987	28.20 ± 0.01	60.87 ± 1.73	12.8 ± 0.4	V
CH-10-60	−24.03121	−65.72095	4764	2.8	1.6	2.6	Granite	0.9	0.985	27.40 ± 0.01	60.23 ± 1.54	12.0 ± 0.3	V
CH-10-62	−24.03463	−65.72215	4683	4.1	3.5	1.9	Granite	1.4	0.986	26.40 ± 0.01	57.87 ± 1.53	12.0 ± 0.3	V
CH-10-59	−24.03100	−65.72105	4765	5.3	4.9	2.3	Granite	1.0	0.985	26.80 ± 0.01	58.10 ± 1.52	11.6 ± 0.3	V

[a] Analytical (internal) uncertainty.

surface, and the boulders heights (0.8–0.6 m) far above the moraine matrix would imply they were not buried.

Excluding the two mentioned outliers, the ages on MG I are older than MG II (except for boulder CH-10-83), which are in agreement with the relative positions of the moraines (Fig. 3A). Despite some scattering in the ages and current uncertainties associated with scaling in a pre-LGM timeframe, we can still confidently state that 6 ages from MG I and II indicate glacial activity between ~52 and ~39 ka, during Marine Isotopic Stage 3 (MIS 3).

4.2.2. MG III

On both sides of Nevado de Chañi 17 boulders were dated from MG III. Two of them from the east side are obvious outliers, more than 20 ka older than the rest (CH-10-55 and CH-12-78) and represent a prior period of exposure (inheritance). On the east side, boulders arise from 2 lateral and 2 frontal moraines (Fig. 3B). The four boulders from the external lateral moraine (CH-10-48 to 51) have ages between 25 and 22.3 ka (Fig. 7A). The internal lateral moraine (CH-10-44 to 47), located ~120 m inboard, has exposure ages that overlap at ±1σ with the external lateral moraine except

for the sample CH-10-45 (17.8 ± 0.5 ka; Fig. 7B). Without considering CH-10-45, 7 samples of the lateral moraine (internal and external combined) form a cluster from 25 to 21 ka, with a peak of 24.7 and a mean of 23.5 ± 1.4 ka (Fig. 7C). The data do not allow us to distinguish an age difference between the inner and the outer lateral moraines within uncertainties (Figs. 3B and 7C).

Also on the east side, a frontal moraine shows three scattered ages that range between 22.3 and 16.2 ka (Figs. 3B and 7D). According to its position, and the age of the lateral moraines that it links to (i.e., lateral-frontal), we infer the moraine age is likely represented by sample CH-10-56 (22.3 ka). Regardless, our findings are not affected by the scatter and lack of a defining age for this sliver of frontal moraine crest.

On the west side, four boulders have been dated on MG III. The ages range from 24.8 to 14.9 ka. Three boulders are between 24.8 and 18.8 ka. The youngest boulder of 14.9 ka is considered an outlier given the other 3 ages and it does not represent the MG III age distribution (Fig. 7). Interestingly, the youngest boulder (14.9 ka) has the same age as the inboard and thus younger MG IV (see below). It could be reflecting post-depositional disturbance during the later MG IV timeframe deposition.
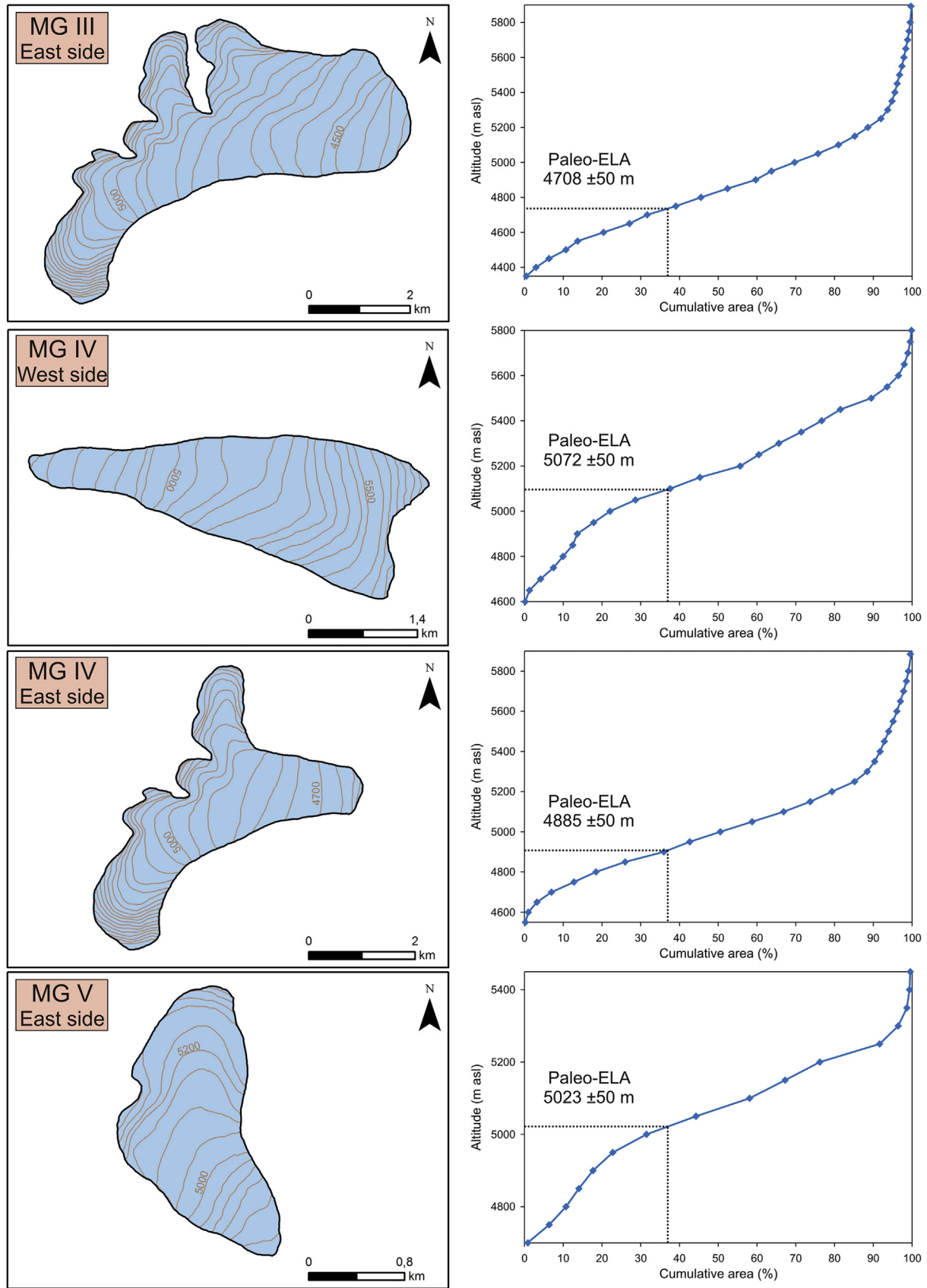
Fig. 6. Paleo-equilibrium line reconstructions. Paleoglacier extent surface reconstruction (left) and the hypsometric curve (cumulative area vs altitude; right) for the calculation of paleo-ELA using the AAR approach. We use an AAR = 0.67 (right) although this does not affect our main conclusions. The paleo-ELA of MG IV from west side was calculated in the Quebrada Chañi Sur valley (Fig. 3).
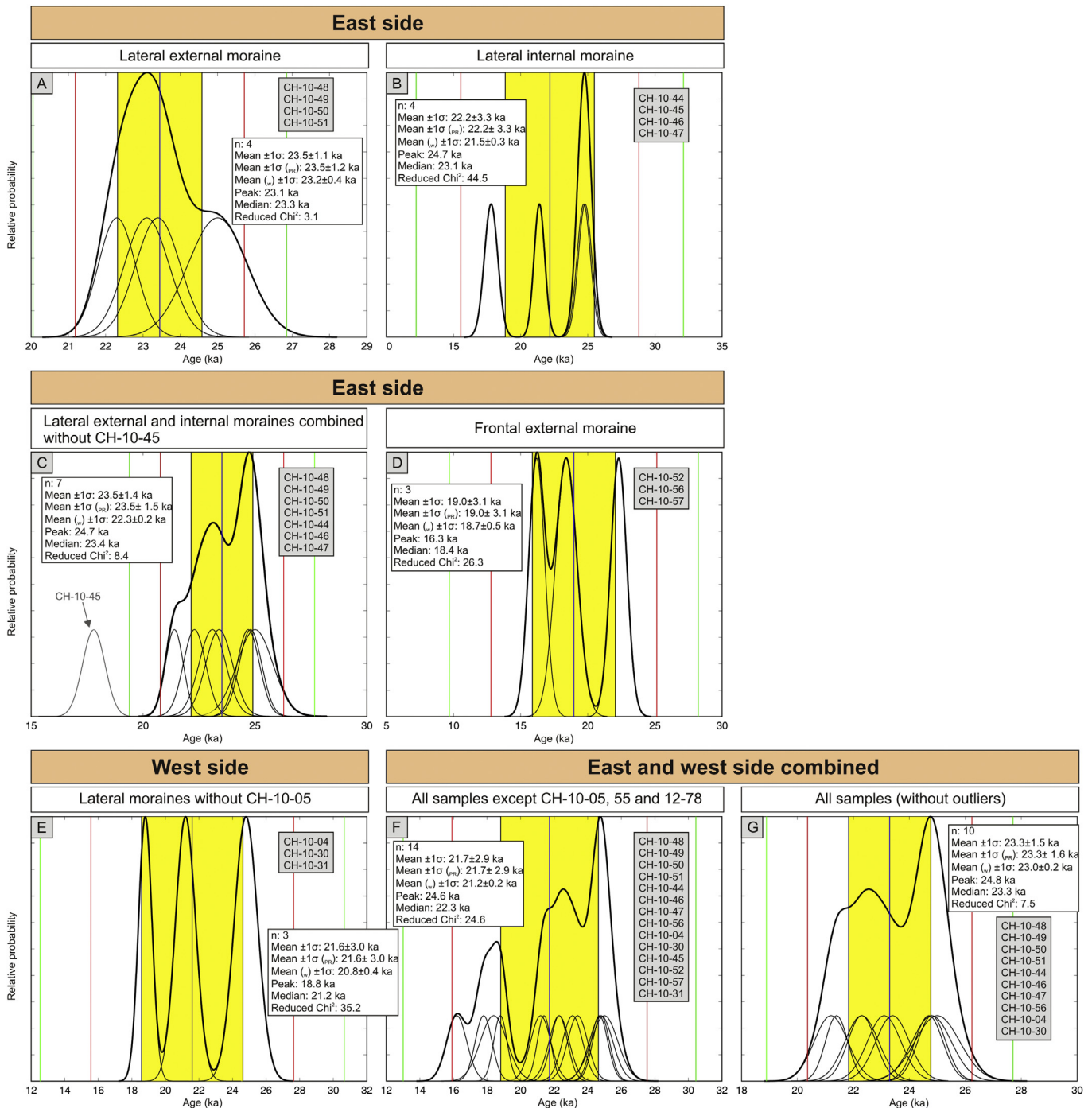
Fig. 7. Probability density functions ('camel plots') for MG III (with and without outliers). Individual ages are shown by thin black lines with the analytical (internal) uncertainty (±1σ). The thick black line represents the probability distribution of the representative age population. Ages are shown grouped by moraine crest and valley (A to E) and all samples together (F and G). In C, one outlier (CH-10-45) is shown in grey color and it was not included in the calculations. Samples ID and statistics are in inset. Statistics include: arithmetic mean with ±1σ, arithmetic mean with ±1σ and production rate (PR) uncertainty propagated (2.4%), weighted mean (w) with weighted uncertainty, peak age, median and reduced Chi². Black, red and green vertical lines mark ±1σ, ±2σ, and ±3σ from the arithmetic mean, respectively. The center vertical blue line and yellow band denotes the arithmetic mean value ±1σ. (For interpretation of the references to colour in this figure legend, the reader is referred to the web version of this article.)

4.2.2.1. Summary of all MG III ages. Not considering the three above mentioned outliers CH-10-05 (14.9 ± 0.5 ka), CH-10-55 (46.4 ± 0.8 ka) and CH-12-78 (152.7 ± 2.4 ka), the average age of MG III is 21.7 ka. Ten of the remaining 14 MG III ages on east and west sides form a cluster around 25 to 21 ka (Fig. 7F and G). The four other boulders, which are located in different moraine crests on both sides of the massif, yield younger ages (Fig. 7F); moreover, the sample CH-10-57

age (16.2 ± 0.6 ka) overlaps at 1σ with 3 different ages of MG IV (see below). We interpret these four younger ages as representing post-depositional disturbance; these were not considered when calculating MG III age. The mean age of MG III does not change substantially whether or not these outliers are included (compare Figs. 7F and G).

The 'camel plot' in Fig. 7G shows ages from 25 to 21.2 ka, a main

peak of 24.8 ka, and an average (±1σ) of 23.3 ± 1.6 ka. At 1σ, the peak and mean are indistinguishable. As noted above, we cannot distinguish statistically the different moraine crest ages during this time. Nonetheless, we cannot rule out the MG III moraine is composed of more than one glacial event during the period 25 to 21 ka, which may be reflected in the slight bimodal distribution shown in Fig. 7G. That the ages are from different crests supports there is more than one ice margin position represented within age uncertainties. However, given the moraine crests are indistinguishable in age, our main conclusions are not affected if we summarize the age of MG III as being between ~25 and ~22 ka with an average of 23.3 ± 1.6 ka (Fig. 7G).

It is interesting to note that on each moraine system, MG I, II and III, there are ages (outliers) between ~19 and ~16 ka (6 in total). We cannot rule out the possibility that a glacier readvance during this period of time has somehow generated disturbance of boulders on the older (i.e., based on the relative morpho-stratigraphy) MG I, II and III moraines, but we have no evidence to confirm such a scenario.

4.2.3. MG IV

The MG IV has been dated (n = 13) in four different valleys collectively from both sides of Nevado de Chañi (Figs. 3 and 8). Twelve ages range from 15.5 to 14.3 ka (average 15.0 ± 0.5 ka; Fig. 8E), except for one outlier (CH-10-34; ~21 ka). We infer this one boulder (~6 ka older than the other 12 boulders) reflects preexposure (inheritance). The ages of MG IV in each of the four valleys are statistically indistinguishable and present the same average, mode and median (Fig. 8). The scatter between ages can be

explained by analytical uncertainties alone. Hence, we consider the average of the 12 samples (15.0 ± 0.5 ka) as the age of MG IV.

4.2.4. MG V

Four consistent ages for MG V (with no outliers), which is only detected on the eastern side (Fig. 3), provide an age range from 12.8 to 11.6 ka (Fig. 9). The insignificant scatter between ages can be
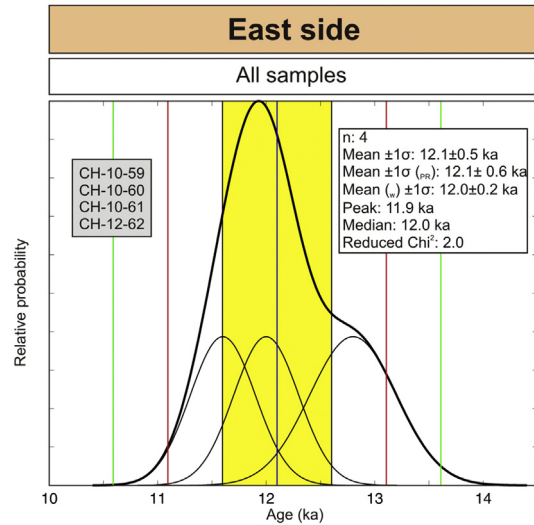
Fig. 9. Similar to Fig. 7, but probability density function for MG V.
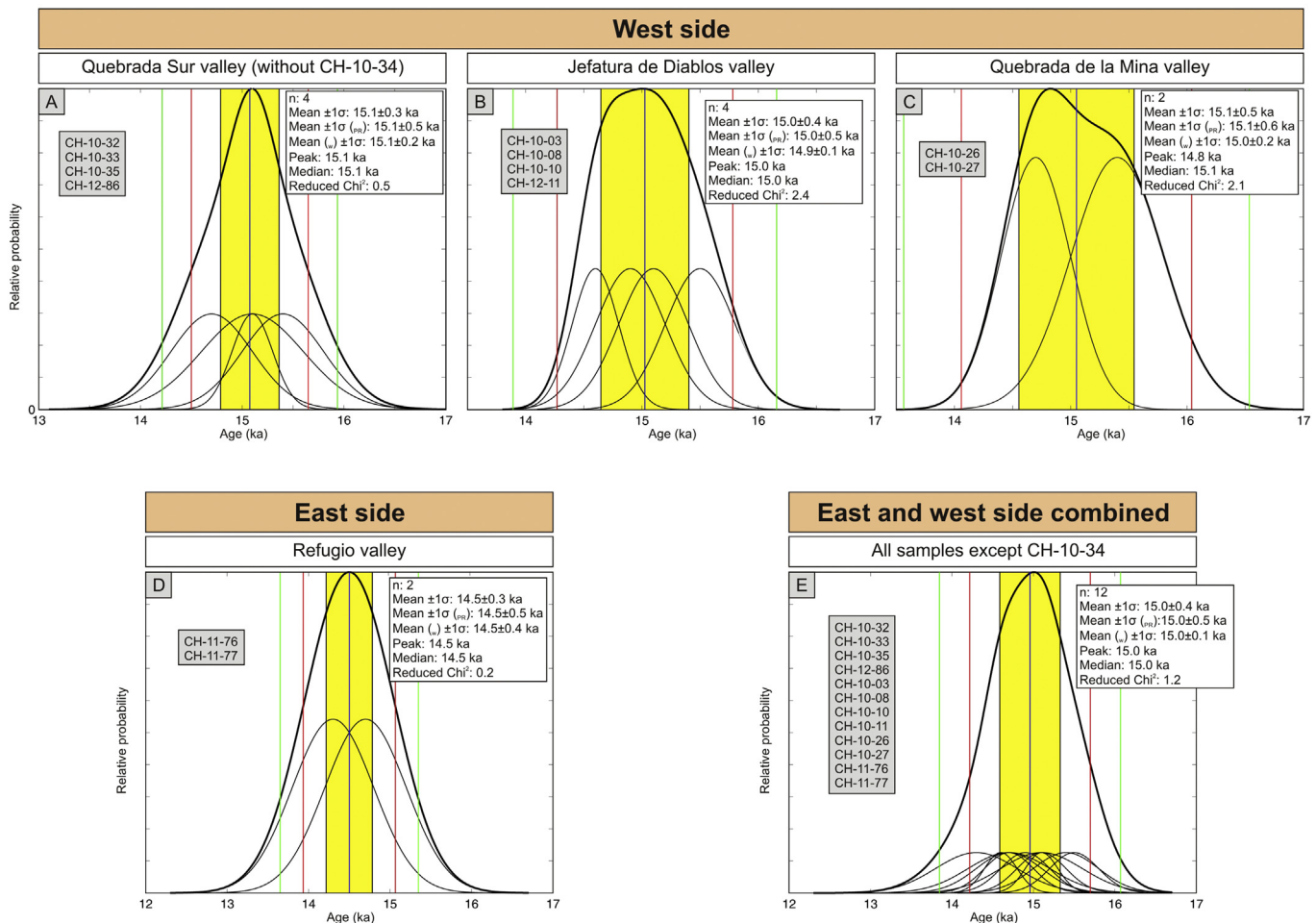
Fig. 8. Similar to Fig. 7, but probability density functions for MG IV (without outlier CH-10-34). Ages are shown grouped by valley (A to D) and all samples together (E).

explained by internal uncertainties alone. Hence, the average of these four ages marks the age of the MG V (12.1 ± 0.6 ka).

4.3. Glacial history and paleo-ELA reconstruction

The oldest glacial deposits around Nevado de Chañi are represented by MG I and II. According to our chronology, MG I and II were

deposited between ~52 and ~39 ka. After that, an important glacial advance on the east side, which is less represented on the west side, took place at 23.3 ± 1.6 ka, leading to deposition of MG III. As the age of MG III was obtained from boulders on different moraine crests on the east side, it is possible that its formation represents more than one glacier pulse to a similar position. On the east side, the paleo-ELA from MG III is located at 4708 ± 50 m asl (Fig. 6). It is
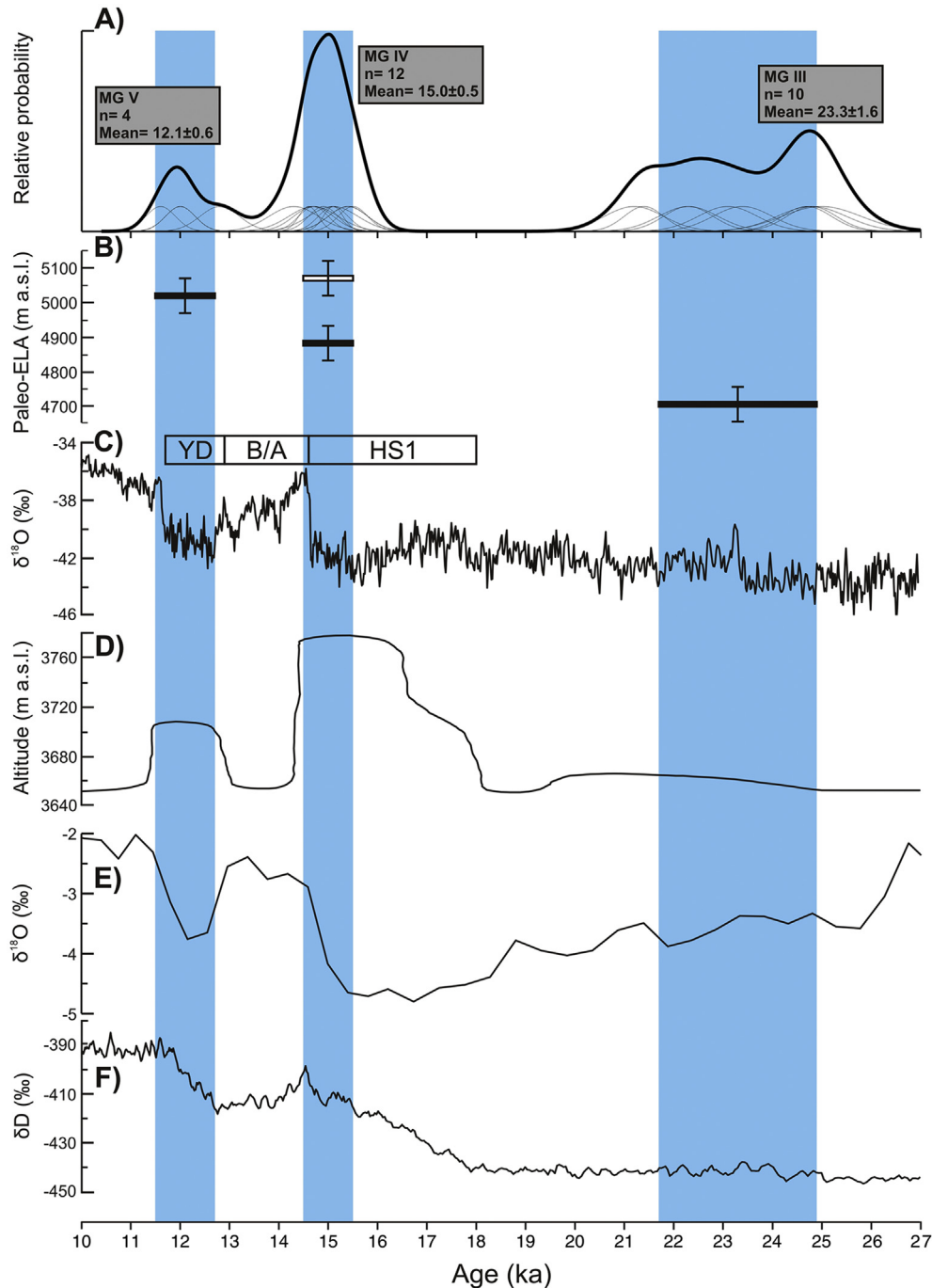
Fig. 10. Glacial chronology of Nevado de Chañi compared with other paleoclimatic records. A) Probability plots of ¹⁰Be ages of MG III, IV and V (without outliers). Thin lines represent individual ages (with ±1σ analytical uncertainty) and thick line the summed distribution. Vertical columns (in blue) indicate the mean age of each moraine including propagation of both analytical and production rate uncertainty (±1σ), as explained in the Methods, Section 3.2. B) Paleo-ELA from the east (black) and west side (white) of Nevado de Chañi, from Fig. 6. Note for MG IV, ELA is constructed for both sides allowing a comparison for this time period. C) NGRIP δ¹⁸O record (Rasmussen et al., 2006) placed in timescale of Lemieux-Dudon et al. (2010). YD: Younger Dryas stadial, D/A: Bølling-Allerød, HS1: Heinrich stadial 1. D) Lake level curve of Altiplano paleolakes (Placzek et al., 2006). E) δ¹⁸O of speleothem record from Boyuverá cave (27°S), southern Brazil (Wang et al., 2007). F) Dome C δD record (EPICA, 2004) placed in timescale of Lemieux-Dudon et al. (2010). (For interpretation of the references to colour in this figure legend, the reader is referred to the web version of this article.)

not possible to estimate a MG III paleo-ELA on the west side due to the limited morphology, specifically the absence of frontal moraines.

Subsequently, at Nevado de Chañi the ELA rose and glaciers retreated, prior to ~15 ka. This recession was then interrupted by two moraine-building events, at 15.0 ± 0.5 ka (MG IV) on both sides, and at 12.1 ± 0.6 ka (MG V), which is only represented on the east side. The ELA increased on the east side by ~180 m from MG III to IV and 140 m from MG IV to V (Fig. 6). The ELA of the ~15 ka glacial expansion was located at 4885 ± 50 m asl on the east side and at 5072 ± 50 m asl on the west side; from this, we observe the ELA was ~190 m higher on the west side of Nevado de Chañi at ~15 ka.

5. Discussion

5.1. Possible climatic factors involved in glacial fluctuations at Nevado de Chañi

The pattern of paleo-ELA, with an increase from east to west across the massif, suggests that the glaciers located on the east side received more precipitation; this pattern existed at least during formation of MG III at the global LGM, and subsequently during MG IV (Fig. 10B). The east to west increase in paleo-ELA confirms that the humidity trajectory and general climate patterns during glaciations were similar to today, that is, from the east-northeast (Fig. 1). A similar pattern been previously reported northward of Nevado de Chañi from Peruvian and Bolivian Andes (Klein et al., 1998; Porter, 2001). The ages and paleo-ELA pattern thus imply that the SASM climate regime continued to influence the South American subtropics during Ice Age climates, such as during the LGM. We infer that if the Southern Hemisphere Westerlies had driven climatic and hydrologic changes in the subtropics in contrast, Ice Age ELAs would instead decrease towards the west.

Because precipitation at Nevado de Chañi is related with the SASM and occurs during the austral summer, we infer some additional climatic factors that can contribute to glacier changes at this site. First, increased snowfall contributes to a positive mass balance in itself. Moreover, snowfall causes higher albedo and is associated with cloudiness, reducing net summer solar radiation received, which is especially important for high-altitude glaciers. Cloudiness and precipitation (i.e., snow), therefore, can reduce the glacier surface temperature and the thermal balance during the summer months. For example, over the much wetter southern Amazon Basin July (winter) is warmer than January (summer), that is, during the mature phase of the SASM. This behavior is explained by the summer time development of clouds (shading the surface from sunlight) and rainfall (moistening the surface) over the central part of South America (Garreaud et al., 2009). Modern climate data from the Altiplano also suggest a similar relationship, with the air temperature being lower at sites with higher precipitation and cloud cover (Placzek et al., 2013) as they reduce solar radiation received. For a high-altitude arid glacier of the Himalaya, Aizen et al. (2002) determined that the incoming solar radiation during the summer months is half that which is theoretically possible because of cloudiness. On the other hand, increased albedo by snowfall has a critical role on the mass balance of high-altitude glaciers that are influenced by monsoons; that is, precipitation changes the surface conditions from glacier ice to snow, slowing down the ablation rates (e.g., Sicart et al., 2005; Azam et al., 2014). Consequently, sublimation and melting are reduced, which are important forcings of the glacier mass balance in such a dry high-altitude environment (Sagredo and Lowell, 2012; Vargo and Galewsky, 2014). Both effects described above could have a major impact on the snow accumulation and preservation at high-altitude sites, favoring glaciers expansions during cooler and higher precipitation periods. Below, we present independent evidence of precipitation changes at the times of moraine building events at Nevado de Chañi.

5.2. Chronology of subtropical changes

To help place the new record into a wider regional paleoclimate context during the last glaciation and subsequent transition to the current interglacial, we review and also compare it to other low-latitude South American archives. Moraines on both sides of Nevado de Chañi (MG I and II) show more extensive glaciations prior to the global LGM, at least during ~52–39 ka, a finding similar to that of other studies in the subtropical Andes (Zech et al., 2009; Blard et al., 2009, 2014; Ward et al., 2015) and in the Southern Hemisphere in general (e.g., Kelley et al., 2014). Although our ages represent a good start, these features cannot be placed in a robust geochronological context without more data. Recalculated previously-obtained [10]Be ages from the tropical Andes by Bromley et al. (2016) suggest that the full glacial conditions occurred before the global LGM, during MIS 3. A tentative correlation can be made with Uturuncu volcano (22°S) and Chajnantor Plateau (23°S) in the Altiplano (Fig. 1), where moraine and striated bedrock indicate glacial activity during ~60–40 ka and ~65–37 ka, respectively (Blard et al., 2014; Ward et al., 2015).

A major glacial advance occurred at ~23 ka (MG III), in phase with the global LGM and the expansions of ice-sheets and mountain glaciers world-wide. Recently published [10]Be ages from Peruvian Andes (Bromley et al., 2016; Shakun et al., 2015) also reveal glacial activity during the global LGM. Due to some scattering in the ages, we cannot precisely establish when the deglaciation started on Nevado de Chañi. Subsequently, a glacial expansion at Nevado de Chañi, corresponding to the MG IV limit, occurred at 15.0 ± 0.5 ka. The MG IV age has been observed in other glacier records in the subtropical Andes (Clapperton et al., 1997; Zech et al., 2009; Blard et al., 2009, 2014) (Fig. 1); as well, it is similar in timing to the Tauca paleolake event on the Bolivian Altiplano (18–14 ka) (Placzek et al., 2006). In turn, glacial activity on the subtropical Andes during the MG V deposition (12.1 ± 0.6 ka) is only reported on the Tunupa volcano (Blard et al., 2009, 2013a). For the rest of the sites shown on Fig. 1, there are no reported glaciers during MG V time or after, indicating the ELAs remained above the elevation of these ranges.

Moreover, we specifically compare the new Nevado de Chañi glacial record to low-latitude lake and caves records, which are particularly sensitive to paleoprecipitation changes. Sediment core records from the Uyuni salt lake reveal a humid phase between 46 and 36 ka (Baker et al., 2001a; Fritz et al., 2004), which can be correlated with MG I and II times. Although there is no firm consensus regarding LGM precipitation changes throughout the low-latitudes, available evidence over the nearby arid Altiplano suggests it was only slightly or moderately wetter (e.g., Baker et al., 2001b; Placzek et al., 2006). Paleoshorelines for the Sasji lake expansion (24–20.5 ka) are only ~15 m above the present-day Salar de Uyuni elevation (Placzek et al., 2006) (Fig. 10).

After the global LGM, during the glacial to interglacial transition, the glacial activity at Nevado de Chañi coincided with periods of high lake levels across the closed-watersheds of the Central Altiplano (Placzek et al., 2006; Blard et al., 2011). The Tauca (18–14 ka) and Coipasa (13–11 ka) cycles correspond with MG IV (15.0 ± 0.5 ka) and V (12.1 ± 0.6 ka), respectively (Fig. 10E). During the Tauca and Coipasa cycles the lake levels were situated at 112 and 42 m, respectively, above the present-day Salar de Uyuni elevation. Moreover, during MG IV and V formation wetter conditions are recorded also in the lowlands of South America, in southern Brazilian speleothems of the Botuverá cave (Wang et al., 2007) (Fig. 10).

We infer the available evidence supports a role for both temperature and precipitation controls on glacial expansions in this part

of the arid subtropical Andes in the past (Fig. 10). On the one hand, glacial expansions around Nevado de Chañi are contemporaneous with wetter periods (of different magnitudes) in the subtropical Andes, especially during the glacial to interglacial transition. This comparison supports the idea that the glaciers at Nevado de Chañi were sensitive to precipitation shifts in the past, in agreement with the present-day observations. On the other hand, a major glacial advance occurred at ~23 ka (MG III) when the lowland tropics and subtropics of South America were ~5 °C cooler than present (e.g., Stute et al., 1995), in phase with the global LGM, and when precipitation was only slightly or moderate higher (Placzek et al., 2006). Moreover, even during the glacial to interglacial transition, glacial and hydrological models reveal a cooling of 5—7 °C as well as a precipitation increase by a factor of 1.6—3 compared to the present values in the nearly Altiplano are needed to drive the Tauca paleo-lake highstand (Blard et al., 2009; Placzek et al., 2013). Last, as discussed in Section 5.1, modern observations reveal that precipitation and temperature change interdependently in high-altitude environments such as the Nevado de Chañi.

5.3. Inferred links with far field changes

After the global LGM, during the transition between glacial and interglacial conditions, polar temperature records in the Northern and Southern Hemispheres show asynchronous changes (Fig. 10). Denton et al. (2010) proposed that the last Termination initiated due the combination of higher summer insolation and the growth in "excess" of the North Hemisphere ice sheet (Raymo, 1997). During the Heinrich stadial 1 (HS1) and Younger Dryas stadial (YD) the North Atlantic sea surface temperature dropped significantly and Atlantic meridional overturning circulation was curtailed (McManus et al., 2004; Barker et al., 2009; Denton et al., 2010) in response to high amounts of meltwater and icebergs from Laurentide and European glaciers. This (winter) cooling in the North Atlantic pushed the ITCZ southward, which would have intensified the SASM and increasing precipitation in the Central Andes (Placzek et al., 2006; Kanner et al., 2012; Quade et al., 2008) and Brazil lowlands (Wang et al., 2004, 2007; Stríkis et al., 2015). Recent records from West Antarctica (Marcott et al., 2014) suggest that the interruption of the Atlantic meridional overturning circulation had a critical role in controlling atmospheric CO_2 rise during the last deglaciation, which could have caused warming in the Southern latitudes when the northern latitudes cooled. Taken at face value, the 15.0 ± 0.5 ka (MG IV) and 12.1 ± 0.6 ka (MG V) glacial expansions roughly coincide with HS1 and YD, respectively. Regarding the former, within error, MG IV occurred towards the end of HS1, especially if it is considered the advance started before the moraine formed. Other studies have also placed the Tauca and Coipasa cycles as coeval with HS1 and YD, respectively (Fig. 10) (Placzek et al., 2006; 2013; Blard et al., 2011). Even given the age uncertainties, the glacial expansion that formed MG IV was well before the maximum extent of Late Glacial advances, ~14—13 ka, recorded in the southernmost part of the continent (Strelin et al., 2011; García et al., 2012). The deglacial HS1 and YD correlations suggest that abrupt climate events initiated in the North Atlantic could have influenced, through curtained Atlantic meridional overturning circulation and impacts on low latitude atmospheric-ocean interactions, the glacial activity at least as far as south as 24°S at Nevado de Chañi.

6. Conclusions

Glacier expansions on Nevado de Chañi occurred during the pre-LGM (~52 —39 ka, MIS 3), the LGM (23.3 ± 1.6 ka), and in two pulses during the last glacial to interglacial transition (15.0 ± 0.5 and 12.1 ± 0.6 ka). Moraine records show different magnitudes of glacial response to climate changes on respective sides of Nevado de Chañi with lower paleo-ELAs in the east (wetter) than on the west (drier) side of the massif. This suggests a moisture trajectory similar as the present, related with the SASM and climates originated from the Atlantic side of the continent. The glacial advance at ~23 ka indicates a major expansion during the global LGM when tropical and subtropical Andes were cooler. Even given age uncertainties, the timing of ~15 ka and ~12 ka events correlates with cooler and wetter periods in the Central Andes (due to the southward shift of the SASM), and cool periods in North Atlantic; for comparison, these are warming periods in Patagonia and Antarctica (Fig. 10). Our findings support a role of temperature as well as precipitation for glacial expansions in this arid sector of the subtropical Andes. We infer climate changes over this part of the Andes could be influenced by changes in the North Atlantic region that impacted low latitude atmospheric-ocean interactions such as the ITCZ and consequently the SASM.

References

Aizen, V.B., Aizen, E.M., Nikitin, S.A., 2002. Glacier regime on the northern slope of the Himalaya (Xixibangma glaciers). Quat. Int. 97—98, 27—39. http://dx.doi.org/10.1016/S1040-6182(02)00049-6.

Ammann, C., Jenny, B., Kammer, K., Messerli, B., 2001. Late quaternary glacier response to humidity changes in the arid Andes of Chile (18-29°S). Palaeogeogr. Palaeoclimatol. Palaeoecol. 172, 313—326. http://dx.doi.org/10.1016/S0031-0182(01)00306-6.

Azam, M.F., Wagnon, P., Vincent, C., Ramanathan, A.L., Favier, V., Mandal, A., Pottakkal, J.G., 2014. Processes governing the mass balance of Chhota Shigri Glacier (western Himalaya, India) assessed by point-scale surface energy balance measurements. Cryosphere 8, 2195—2217. http://dx.doi.org/10.5194/tc-8-2195-2014.

Baker, P.A., Rigsby, C.A., Seltzer, G.O., Fritz, S.C., Lowenstein, T.K., Bacher, N.P., Veliz, C., 2001a. Tropical climate changes at millennial and orbital timescales on the Bolivian Altiplano. Nature 409, 698—701. http://dx.doi.org/10.1038/35055524.

Baker, P.A., Dunbar, R.B., Cross, S.L., Seltzer, G.O., Grove, M.J., Rowe, H.D., Fritz, S.C., Tapia, P.M., Broda, J.P., 2001b. The history of South american tropical precipitation for the past 25,000 years. Science 291, 640—643. http://dx.doi.org/10.1126/science.291.5504.640.

Baker, P.A., Fritz, S.C., 2015. Nature and causes of Quaternary climate variation of tropical South America. Quat. Sci. Rev. 124, 31—47. http://dx.doi.org/10.1016/j.quascirev.2015.06.011.

Balco, G., Stone, J.O., Lifton, N.A., Dunai, T.J., 2008. A complete and easily accessible means of calculating surface exposure ages or erosion rates from [10]Be and [26]Al measurements. Quat. Geochronol. 3, 174—195. http://dx.doi.org/10.1016/j.quageo.2007.12.001.

Barker, S., Diz, P., Vautravers, M.J., Pike, J., Knorr, G., Hall, I.R., Broecker, W.S., 2009. Interhemispheric Atlantic seesaw response during the last deglaciation. Nature 457, 1097—1102. http://dx.doi.org/10.1038/nature07770.

Bianchi, A.R., Yañez, C.E., 1992. Las precipitaciones en el noroeste argentino. INTA Estación Experimental Agropecuaria, Salta, 393pp.

Blard, P.-H., Lavé, J., Sylvestre, F., Placzek, C.J., Claude, C., Galy, V., Condom, T., Tibari, B., 2013a. Cosmogenic [3]He production rate in the high tropical Andes (3800 m, 20° S): implications for the local last glacial maximum. Earth Planet. Sci. Lett. 377, 260—275.

Blard, P.-H., Braucher, D., Lavé, R., Bourlès, J., 2013b. Cosmogenic [10]Be production rate calibrated against [3]He in the high Tropical Andes (3800—4900 m, 20—22° S). Earth Planet. Sci. Lett. 382, 140—149.

Blard, P.H., Lavé, J., Farley, K.A., Fornari, M., Jiménez, N., Ramirez, V., 2009. Late local glacial maximum in the Central Altiplano triggered by cold and locally-wet conditions during the paleolake Tauca episode (17-15 ka, Heinrich 1). Quat. Sci. Rev. 28, 3414—3427. http://dx.doi.org/10.1016/j.quascirev.2009.09.025.

Blard, P.H., Lave, J., Farley, K.A., Ramirez, V., Jimenez, N., Martin, L.C.P., Charreau, J., Tibari, B., Fornari, M., 2014. Progressive glacial retreat in the Southern Altiplano (Uturuncu volcano, 22°S) between 65 and 14 ka constrained by cosmogenic [3]He dating. Quat. Res. 82, 209–221. http://dx.doi.org/10.1016/j.yqres.2014.02.002.

Blard, P.H., Sylvestre, F., Tripati, A.K., Claude, C., Causse, C., Coudrain, A., Condom, T., Seidel, J.L., Vimeux, F., Moreau, C., Dumoulin, J.P., Lavé, J., 2011. Lake highstands on the Altiplano (tropical Andes) contemporaneous with Heinrich 1 and the younger Dryas: new insights from ^{14}C, U-Th dating and δ^{18}O of carbonates. Quat. Sci. Rev. 30, 3973–3989. http://dx.doi.org/10.1016/j.quascirev.2011.11.001.

Borchers, B., Marrero, S., Balco, G., Caffee, M., Goehring, B., Lifton, N., Nishiizumi, K., Phillips, F., Schaefer, J., Stone, J., 2016. Geological calibration of spallation production rates in the CRONUS-Earth project. Quat. Geochronol. 31, 188–198. http://dx.doi.org/10.1016/j.quageo.2015.01.009.

Bromley, G.R.M., Schaefer, J.M., Hall, B.L., Rademaker, K.M., Putnam, A.E., Todd, C.E., Hegland, M., Winckler, G., Jackson, M.S., Strand, P.D., 2016. A cosmogenic [10]Be chronology for the local last glacial maximum and termination in the Cordillera Oriental, southern Peruvian Andes: implications for the tropical role in global climate. Quat. Sci. Rev. 148, 54–67. http://dx.doi.org/10.1016/j.quascirev.2016.07.010.

Casassa, G., Haeberli, W., Jones, G., Kaser, G., Ribstein, P., Rivera, A., Schneider, C., 2007. Current status of Andean glaciers. Glob. Planet. Change 59, 1–9. http://dx.doi.org/10.1016/j.gloplacha.2006.11.013.

Clapperton, C.M., Clayton, J.D., Benn, D.I., Marden, C.J., Argollo, J., 1997. Late Quaternary glacier advances and palaeolake highstands in the Bolivian Altiplano. Quat. Int. 38/39, 49–59. http://dx.doi.org/10.1016/S1040-6182(96)00020-1.

Clark, P.U., Dyke, A.S., Shakun, J.D., Carlson, A.E., Clark, J., Wohlfarth, B., Mitrovica, J.X., Hostetler, S.W., McCabe, A.M., 2009. The last glacial maximum. Science 325, 710–714. http://dx.doi.org/10.1126/science.1172873.

Denton, G.H., Anderson, R.F., Toggweiler, J.R., Edwards, R.L., Schaefer, J.M., Putnam, A.E., 2010. The last glacial termination. Science 328, 1652–1656. http://dx.doi.org/10.1126/science.1184119.

Douglass, D.C., Singer, B.S., Kaplan, M.R., Mickelson, D.M., Caffee, M.W., 2006. Cosmogenic nuclide surface exposure dating of boulders on last-glacial and late-glacial moraines, Lago Buenos Aires, Argentina: interpretive strategies and paleoclimate implications. Quat. Geochronol. 1, 43–58. http://dx.doi.org/10.1016/j.quageo.2006.06.001.

EPICA, 2004. Eight glacial cycles from an Antarctic ice core. Nature 429, 623–628.

Fritz, S.C., Baker, P.A., Lowenstein, T.K., Seltzer, G.O., Rigsby, C.A., Dwyer, G.S., Tapia, P.M., Arnold, K.K., Ku, T.L., Luo, S., 2004. Hydrologic variation during the last 170,000 years in the southern hemisphere tropics of South America. Quat. Res. 61, 95–104. http://dx.doi.org/10.1016/j.yqres.2003.08.007.

García, J.L., Kaplan, M.R., Hall, B.L., Schaefer, J.M., Vega, R.M., Schwartz, R., Finkel, R., 2012. Glacier expansion in Southern Patagonia throughout the antarctic cold reversal. Geology 40, 859–862. http://dx.doi.org/10.1130/G33164.1.

Garreaud, R.D., Vuille, M., Compagnucci, R., Marengo, J., 2009. Present-day South American climate. Palaeogeogr. Palaeoclimatol. Palaeoecol. 281, 180–195. http://dx.doi.org/10.1016/j.palaeo.2007.10.032.

González, M.A., Tchilinguirian, P., Pereyra, F., Ramallo, E., Gonzalez, O.E., 2004. Hoja Geológica 2366-IV Ciudad de Libertador General San Martín, provincias de Jujuy y Salta: SEGEMAR scale 1:250.000, 1 sheet, 114 pp text.

Haselton, K., Hilley, G., Strecker, M.R., 2002. Average pleistocene climatic patterns in the southern central Andes: controls on mountain glaciation and paleoclimate implications. J. Geol. 110, 211–226. http://dx.doi.org/10.1086/338414.

Hermanns, R.L., Niedermann, S., Villanueva, G.A., Schellenberger, A., 2006. Rock avalanching in the NW Argentine Andes as a result of complex interactions of lithologic, structural and topographic boundary conditions, climate change and active tectonics. In: Evans, S.G., Scarascia-Mugnozza, G., Strom, A.L., Hermanns, R.L. (Eds.), Massive Rock Slope Failure: New Models for Hazard Assessment, pp. 497–520.

Jordan, E., 1991. Die Gletscher der bolivianischen Anden. Franz Steiner Verlag, Stuttgart, Germany, 365pp.

Kaplan, M.R., Coronato, A., Hulton, N.R.J., Rabassa, J.O., Kubik, P.W., Freeman, S.P.H.T., 2007. Cosmogenic nuclide measurements in southernmost South America and implications for landscape change. Geomorphology 87, 284–301. http://dx.doi.org/10.1016/j.geomorph.2006.10.005.

Kaplan, M.R., Strelin, J., Schaefer, J.M., Denton, G.H., Finkel, R.C., Schwartz, R., Putnam, A.E., Vandergoes, M.J., Goehring, B.M., Travis, S.G., 2011. In-situ cosmogenic [10]Be production rate at Lago Argentino, Patagonia: implications for late-glacial climate chronology. Earth Planet. Sci. Lett. 309, 21–32. http://dx.doi.org/10.1016/j.epsl.2011.06.018.

Kanner, L.C., Burns, S.J., Cheng, H., Eduards, L., 2012. High-latitude forcing of the South American Summer Monsoon during the last glacial. Science 335, 570–573.

Kelley, S.E., Kaplan, M.R., Schafer, J.M., Andersen, B.G., Barrell, D.J.A., Putnam, A.E., Denton, G.H., Schwartz, R., Finkel, R.C., Doughty, A.M., 2014. High-precision [10]Be chronology of moraines in the Southern Alps indicates synchronous cooling in Antarctica and New Zealand 42,000 years ago. Earth Planet. Sci. Lett. 405, 194–206. http://dx.doi.org/10.1016/j.epsl.2014.07.031.

Kelly, M.A., Lowell, T.V., Applegate, P.J., Phillips, F.M., Schaefer, J.M., Smith, C.A., Kim, H., Leonard, K.C., Hudson, A.M., 2015. A locally calibrated, late glacial [10]Be production rate from a low-altitude, high-altitude site in the Peruvian Andes. Quat. Geochronol. 26, 70–85. http://dx.doi.org/10.1016/j.quageo.2013.10.007.

Klein, A.G., Seltzer, G.O., Isacks, B.L., 1998. Modern and local glacial maximum snowlines in the central Andes of Peru, Bolivia and Northern Chile. Quat. Sci. Rev. 17, 1–21. http://dx.doi.org/10.1016/S0277-3791(98)00095-X.

Lal, D., 1991. Cosmic ray labeling of erosion surfaces: in situ nuclide production rates and erosion models. Earth Planet. Sci. Lett. 104, 424–439. http://dx.doi.org/10.1016/0012-821X(91)90220-C.

Lemieux-Dudon, B., Blayo, E., Petit, J.R., Waelbroeck, C., Svensson, A., Ritz, C., Barnola, J.M., Narcisi, B.M., Parrenin, F., 2010. Consistent dating for Antarctic and Greenland ice cores. Quat. Sci. Rev. 29, 8–20. http://dx.doi.org/10.1016/j.quascirev.2009.11.010.

Lifton, N., Sato, T., Dunai, T.J., 2014. Scaling in situ cosmogenic nuclide production rates using analytical approximations to atmospheric cosmic-ray fluxes. Earth Planet. Sci. Lett. 386, 149–160. http://dx.doi.org/10.1016/j.epsl.2013.10.052.

Lliboutry, L., 1956. La mecanique des glaciers en particulier au voisinage de leur front. Ann. Geophys. 12, 245–276.

Lliboutry, L., 1999. Glaciers of Chile and Argentina. In: Williams Jr., R.J., Ferringo, J.G. (Eds.), Glaciers of South America, pp. 181–206. US Geol. Surv. Prof. Pap. 1386-I.

Marcott, S. a, Bauska, T.K., Buizert, C., Steig, E.J., Rosen, J.L., Cuffey, K.M., Fudge, T.J., Severinghaus, J.P., Ahn, J., Kalk, M.L., McConnell, J.R., Sowers, T., Taylor, K.C., White, J.W.C., Brook, E.J., 2014. Centennial-scale changes in the global carbon cycle during the last deglaciation. Nature 514, 616–619. http://dx.doi.org/10.1038/nature13799.

Martin, L.C.P., Blard, P.-H., Lavé, J., Braucher, R., Lupker, M., Condom, T., Charreau, J., Mariotti, V., Davy, E., 2015. In situ cosmogenic [10]Be production rate in the High Tropical Andes. Quat. Geochronol. 30, 54–68. http://dx.doi.org/10.1016/j.quageo.2015.06.012.

Martini, M.A., Strelin, J.A., Astini, R.A., 2015. Distribución y caracterización de la geomorfología glaciar en la Cordillera Oriental de Argentina. Acta Geol. lilloana 27, 105–120.

Martini, M.A., Strelin, J.A., Astini, R.A., 2013. Inventario y caracterización morfoclimática de los glaciares de roca en la Cordillera Oriental Argentina (entre 22° y 25° S). Rev. Mex. Ciencias Geol. 30, 569–581.

McManus, J.F., Francois, R., Gherardi, J.-M., Keigwin, L.D., Brown-Leger, S., 2004. Collapse and rapid resumption of Atlantic meridional circulation linked to deglacial climate changes. Nature 428, 834–837. http://dx.doi.org/10.1038/nature02494.

Members, W.D.P., 2015. Precise interpolar phasing of abrupt climate change during the last ice age. Nature 520, 661–665. http://dx.doi.org/10.1038/nature14401.

Milana, J.P., 2012. El Continuum del ambiente glacial y la importancia del contenido sedimentario. In: Proceeding of the XIII Reunión Argentina de Sedimentología, pp. 140–141. Salta, Argentina.

Nishiizumi, K., Imamura, M., Caffee, M.W., Southon, J.R., Finkel, R.C., McAninch, J., 2007. Absolute calibration of [10]Be AMS standards. Nucl. Instrum. Methods Phys. Res. Sect. B Beam Interact. Mat. Atoms 258, 403–413. http://dx.doi.org/10.1016/j.nimb.2007.01.297.

Pedro, J.B., Van Ommen, T.D., Rasmussen, S.O., Morgan, V.I., Chappellaz, J., Moy, A.D., Masson-Delmotte, V., Delmotte, M., 2011. The last deglaciation: timing the bipolar seesaw. Clim. Past. 7, 671–683. http://dx.doi.org/10.5194/cp-7-671-2011.

Placzek, C., Quade, J., Patchett, P.J., 2006. Geochronology and stratigraphy of late Pleistocene lake cycles on the southern Bolivian Altiplano: implications for causes of tropical climate change. Bull. Geol. Soc. Am. 118, 515–532. http://dx.doi.org/10.1130/B25770.1.

Placzek, C.J., Quade, J., Patchett, P.J., 2013. A 130 ka reconstruction of rainfall on the Bolivian Altiplano. Earth Planet. Sci. Lett. 363, 97–108. http://dx.doi.org/10.1016/j.epsl.2012.12.017.

Porter, C., 1975. Equilibrium-line altitudes of late quaternary alps, New Zealand glaciers in the southern alps, New Zealand. Quat. Res. 5, 27–47.

Porter, S.C., 2001. Snowline depression in the tropics during the last glaciation. Quat. Sci. Rev. 20, 1067–1091. http://dx.doi.org/10.1016/S0277-3791(00)00178-5.

Putnam, A.E., Schaefer, J.M., Barrell, D.J.A., Vandergoes, M., Denton, G.H., Kaplan, M.R., Finkel, R.C., Schwartz, R., Goehring, B.M., Kelley, S.E., 2010. In situ cosmogenic [10]Be production-rate calibration from the Southern Alps, New Zealand. Quat. Geochronol. 5, 392–409. http://dx.doi.org/10.1016/j.quageo.2009.12.001.

Putnam, A.E., Schaefer, J.M., Denton, G.H., Barrell, D.J.A., Birkel, S.D., Andersen, B.G., Kaplan, M.R., Finkel, R.C., Schwartz, R., Doughty, A.M., 2013. The last glacial maximum at 44°S documented by a [10]Be moraine chronology at lake ohau, southern alps of New Zealand. Quat. Sci. Rev. 62, 114–141. http://dx.doi.org/10.1016/j.quascirev.2012.10.034.

Quade, J., Rech, J.A., Betancourt, J.L., Latorre, C., Quade, B., Rylander, K.A., Fisher, T., 2008. Paleowetlands and regional climate change in the central Atacama Desert, northern Chile. Quat. Res. 69, 343–360. http://dx.doi.org/10.1016/j.yqres.2008.01.003.

Rasmussen, S.O., Andersen, K.K., Svensson, A.M., Steffensen, J.P., Vinther, B.M., Clausen, H.B., Siggaard-Andersen, M.L., Johnsen, S.J., Larsen, L.B., Dahl-Jensen, D., Bigler, M., Röthlisberger, R., Fischer, H., Goto-Azuma, K., Hansson, M.E., Ruth, U., 2006. A new Greenland ice core chronology for the last glacial termination. J. Geophys. Res. Atmos. 111 http://dx.doi.org/10.1029/2005JD006079.

Raymo, M.E., 1997. The timing of major climate terminations. Paleoceanography 12, 577. http://dx.doi.org/10.1029/97PA01169.

Sagredo, E.A., Lowell, T.V., 2012. Climatology of Andean glaciers: a framework to understand glacier response to climate change. Glob. Planet. Change 86–87, 101–109. http://dx.doi.org/10.1016/j.gloplacha.2012.02.010.

Schaefer, J.M., Denton, G.H., Kaplan, M., Putnam, A., Finkel, R.C., Barrell, D.J., Andersen, B.G., Schwartz, R., Mackintosh, A., Chinn, T., Schluchter, C., 2009. High-frequency Holocene glacier fluctuations in New Zealand differ from the northern signature. Science 324, 622–625. http://dx.doi.org/10.1126/

science.1169312.

Schotterer, U., Grosjean, M., Stichler, W., Ginot, P., Kull, C., 2003. Glaciers and climate in the Andes between the equator and 30° S: what is recorded under extreme environmental conditions? Clim. Change 59, 157–175.

Shakun, J.D., Clark, P.U., Marcott, S.A., Brook, E.J., Lifton, N.A., Caffee, M., Shakun, W.R., 2015. Cosmogenic dating of Late Pleistocene glaciation, southern tropical Andes. Peru. J. Quat. Sci. 30, 841–847. http://dx.doi.org/10.1002/jqs.2822.

Sicart, J.E., Wagnon, P., Ribstein, P., 2005. Atmospheric controls of the heat balance of Zongo Glacier (16°S, Bolivia). J. Geophys. Res. D. Atmos. 110, 1–17. http://dx.doi.org/10.1029/2004JD005732.

Stone, J.O., 2000. Air pressure and cosmogenic isotope production. J. Geophys. Res. 105, 23753–23759.

Strecker, M.R., Alonso, R.N., Bookhagen, B., Carrapa, B., Hilley, G.E., Sobel, E.R., Trauth, M.H., 2007. Tectonics and climate of the southern central Andes. Annu. Rev. Earth Planet. Sci. 35, 747–787. http://dx.doi.org/10.1146/annurev.earth.35.031306.140158.

Strelin, J.A., Denton, G.H., Vandergoes, M.J., Ninnemann, U.S., Putnam, A.E., 2011. Radiocarbon chronology of the late-glacial puerto bandera moraines, southern patagonian icefield, Argentina. Quat. Sci. Rev. 30, 2551–2569. http://dx.doi.org/10.1016/j.quascirev.2011.05.004.

Stríkis, N.M., Chiessi, C.M., Cruz, F.W., Vuille, M., Cheng, H., De Souza Barreto, E.A., Mollenhauer, G., Kasten, S., Karmann, I., Edwards, R.L., Bernal, J.P., Sales, H.D.R., 2015. Timing and structure of mega-SACZ events during Heinrich stadial 1. Geophys. Res. Lett. 42, 5477–5484. http://dx.doi.org/10.1002/2015GL064048.

Stute, M., Forster, M., Frischkorn, H., Serejo, A., J,F, C., Schlosser, P., Broecker, W.S., Bonani, G., 1995. Cooling of tropical Brazil (5° C) during the last glacial maximum. Science 269, 379–383.

Trauth, M.H., Alonso, R.A., Haselton, K.R., Hermanns, R.L., Strecker, M.R., 2000. Climate change and mass movements in the NW Argentine Andes. Earth Planet. Sci. Lett. 179, 243–256. http://dx.doi.org/10.1016/S0012-821X(00)00127-8.

Trauth, M.H., Bookhagen, B., Marwan, N., Strecker, M.R., 2003. Multiple landslide clusters record Quaternary climate changes in the northwestern Argentine Andes. Palaeogeogr. Palaeoclimatol. Palaeoecol. 194, 109–121. http://dx.doi.org/10.1016/S0031-0182(03)00273-6.

Vargo, L., Galewsky, J., 2014. Quantifying the change in equilibrium-line altitude during the Last Glacial Maximum in the Subtropical Andes using a mass-balance model. In: American Geophysical Union. Fall Meeting 2014, Abstract #C43A-0371.

Vera, C., 2006. Towards a unified view of the american monsoon system. J. Clim. 19, 5000.

Vuille, M., Burns, S.J., Taylor, B.L., Cruz, F.W., Bird, B.W., Abbott, M.B., Kanner, L.C., Cheng, H., Novello, V.F., 2012. A review of the South American monsoon history as recorded in stable isotopic proxies over the past two millennia. Clim. Past. 8, 1309–1321. http://dx.doi.org/10.5194/cp-8-1309-2012.

Wang, X., Auler, A.S., Edwards, R.L., Cheng, H., Cristalli, P.S., Smart, P.L., Richards, D. a, Shen, C.-C., 2004. Wet periods in northeastern Brazil over the past 210 kyr linked to distant climate anomalies. Nature 432, 740–743. http://dx.doi.org/10.1038/nature03067.

Wang, X., Auler, A.S., Edwards, R.L., Cheng, H., Ito, E., Wang, Y., Kong, X., Solheid, M., 2007. Millennial-scale precipitation changes in southern Brazil over the past 90,000 years. Geophys. Res. Lett. 34, 1–5. http://dx.doi.org/10.1029/2007GL031149.

Ward, D.J., Cesta, J.M., Galewsky, J., Sagredo, E., 2015. Late pleistocene glaciations of the arid subtropical Andes and new results from the Chajnantor Plateau, northern Chile. Quat. Sci. Rev. 128, 98–116. http://dx.doi.org/10.1016/j.quascirev.2015.09.022.

Zappettini, E.O., Coira, B., Santos, O.J., 2008. Edad U/Pb de la Formación Chañi: un granito del arco magmático Tilcárico. In: 17th Congreso Geológico Argentino, Abstractas I, pp. 248–249.

Zech, J., Zech, R., Kubik, P.W., Veit, H., 2009. Glacier and climate reconstruction at Tres Lagunas, NW Argentina, based on 10Be surface exposure dating and lake sediment analyses. Palaeogeogr. Palaeoclimatol. Palaeoecol. 284, 180–190. http://dx.doi.org/10.1016/j.palaeo.2009.09.023.

Zhou, J., Lau, K.M., 1998. Does a monsoon climate exist over South America? J. Clim. 11, 1020–1040. http://dx.doi.org/10.1175/1520-0442(1998)011<1020:DAMCEO>2.0.CO;2.